Hindawi
Neural Plasticity
Volume 2024, Article ID 4784818, 17 pages
https://doi.org/10.1155/2024/4784818

Research Article

Electroacupuncture Therapy Effectively Protects the Rat Brain after Intracerebral Hemorrhage

Li Huang,[1] Xuehui Fan,[2] Yao Chen,[3] Heng Lin,[4] Xiaoqian Jiang,[4] and Chaoxian Yang[2,4,5]

[1]*Department of Anesthesiology, Second Affiliated Hospital of Army Medical University, Chongqing 400037, China*
[2]*Ministry of Education and Medical Electrophysiological Key Laboratory of Sichuan Province, Southwest Medical University, Luzhou 646000, China*
[3]*Department of Pathology, People's Hospital of Chongqing Banan District, Chongqing 401320, China*
[4]*Department of Anatomy, College of Basic Medicine, Southwest Medical University, Luzhou 646000, China*
[5]*Preclinical Medicine Research Center, Southwest Medical University, Luzhou 646000, China*

Correspondence should be addressed to Chaoxian Yang; lyycx@foxmail.com

Received 2 July 2023; Revised 17 December 2023; Accepted 31 January 2024; Published 15 February 2024

Academic Editor: Gabriele Sansevero

Objective. Electroacupuncture (Ea) is a useful complementary and alternative therapy for intracerebral hemorrhage (ICH). However, the neurobiological basis for the Ea treatment of ICH is still unclear. The primary aim of the present study was to explore whether Ea prevents brain edema, apoptosis, excitotoxicity, and neuroinflammation in rats after hemorrhagic stroke. *Methods*. Rats were randomly divided into Sham, Control, and Ea groups. We used modified neurological severity score (mNSS) and gait analysis to estimate neurological function in rats, and PET/CT to assess glucose uptake and the hemorrhagic focus volume. Measurement of the brain water content and TUNEL staining were used to evaluate brain edema and cell apoptosis, respectively. The serum myelin basic protein (MBP), neuron-specific enolase (NSE), calcium-binding protein B (S100B), and tumor necrosis factor-α (TNF-α) concentrations were examined with ELISA. The expression levels of the CD68, GALC, Arg-1, iNOS, NR2A, Glu2R, AQP4, MAP2, GFAP, AQP9, Bcl-2, Bax, and Glu proteins around the hematoma were detected via immunohistochemistry staining. Western blot was used to analyze the levels of the AQP4, AQP9, Bax, Bcl-2, iNOS, and Arg-1 proteins. *Results*. Ea treatment improved neurological function and reduced the hemorrhagic area and brain water content in rats after ICH. The serum concentrations of MBP, NSE, S100B, and TNF-α all decreased significantly in the Ea group compared with the Control group. Expression levels of the Glu, NR2A, AQP4, AQP9, Bax, GFAP, iNOS, and CD68 proteins in brain tissue surrounding the hematoma were obviously suppressed in ICH rats following Ea treatment. Moreover, Ea stimulation increased the levels of the MAP2, GALC, Glu2R, Arg-1, and Bcl-2 proteins, but reduced the number of TUNEL-positive cells in rats after ICH. *Conclusion*. The results of this study suggest that Ea may exert neuroprotective effects by suppressing brain edema, apoptosis, excitotoxicity, and neuroinflammation.

1. Introduction

Intracerebral hemorrhage (ICH), a globally significant cause of death and disability, is one of the most common lethal diseases of the central nervous system (CNS) [1]. The incidence of ICH is increasing year by year, and the average age at morbidity is declining. ICH not only has high mortality and disability rates but also seriously invokes a financial burden on families and society as a whole [2]. Despite notable progress in clinical treatments for ICH, current therapies are still unsatisfactory.

Electroacupuncture (Ea), a combination of traditional acupuncture and modern electrostimulation, is a complementary, alternative therapy for ICH whose use and understanding have developed rapidly in recent decades [3, 4]. Ea is effective for treating a number of conditions, including hyperalgesia, postaccident ICH through the acceleration of angiogenesis, and inflammation following spinal cord injury in rats [4–8]. Our previous research demonstrated that Ea stimulation of the Baihui (GV20) and Dazhui (GV14) acupoints can improve neurological outcomes [9]. Although there is significant evidence that Ea could play a crucial role in ICH

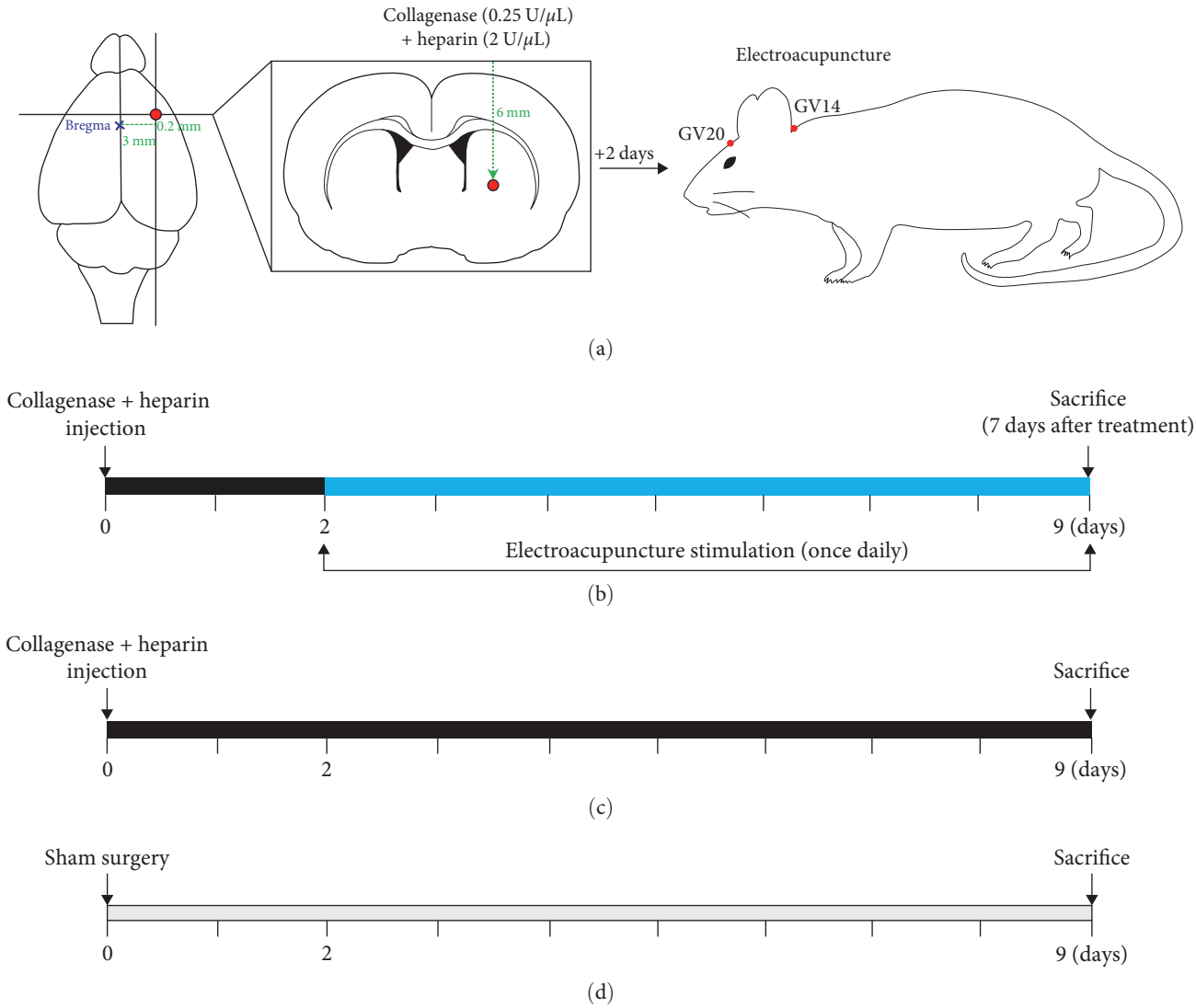

Figure 1: Conceptual description of the experimental protocol. (a) Schematic diagrams of rat ICH models with Ea stimulation. (b–d) Brief timeline of the experimental procedures ((b) Ea group, (c) Control group, and (d) Sham group).

treatment, its mechanism of action is not yet fully understood. Thus, we investigated the effect of Ea on hemorrhagic brain injury and sought to identify the possible mechanisms involved.

2. Materials and Methods

2.1. Animals. Eight to ten week-old adult male specific pathogen free (SPF) Sprague–Dawley (SD) rats weighing 250–300 g were used in this study. All these animals were housed under controlled conditions at $23 \pm 2°C$ under a 12 hr light–dark cycle with free access to food and water. The experimental protocol was approved by the Ethical Committee for Animal Experimental Center of the Southwest Medical University and was in accordance with the guidelines of the People's Republic of China for experimental animals.

2.2. ICH Model. Rats were randomly divided into the following groups: Sham, Control, and Ea. The ICH rats were established, as previously described [10]. Briefly, after anesthetizing by intraperitoneal injection of 2% pentobarbital sodium (2 μL/g), the rats were placed in a stereotaxic frame (Stoelting Co., USA) in the prone position, keeping the anterior and posterior fontanelles at the same level. Following scalp disinfection and longitudinal incision, a burr hole was drilled on the right cranial bone (location: 0.2 mm anterior to the bregma, 3 mm right lateral to the midline), and a Hamilton syringe needle was inserted at a point 6 mm vertical and ventral to the hole was used to inject 2 μL collagenase I (0.125 U/μL) and 1 μL heparin (2 U/μL) at a rate of 0.3 μL/min for 10 min (Figure 1(a)). After 5 min, the needle was slowly removed at a rate of 1 mm/min. After infusion, the borehole was sealed with bone wax, and the scalp was sutured. Rats in the Sham group underwent the same surgical procedure but without the collagenase I and heparin injection.

2.3. Ea Treatment. Two days after ICH, the Ea group began daily Ea stimulation according to our previous methods at the GV20 and GV14 acupoints until sacrifice [9] (Figure 1(b)). One acupuncture needle was obliquely inserted 2 mm into the GV20 acupoint and another was vertically inserted 5 mm into

the GV14 acupoint. Both needles were connected to the type HM6805-II Ea apparatus (SMIF, China). Stimulation was carried out at an intensity of 1 mA, a frequency of 3 Hz, and a stimulation duration of 10 min. The animals in the Control and Sham groups did not receive electrical stimulation (Figures 1(c) and 1(d)).

2.4. Modified Neurological Severity Score (mNSS). The mNSS test was used to assess neurobehavioral deficits through a series of motor, sensory, balance, and reflex measurements [10]. The score of 0–18 indicated the degree of injury (normal score, 0; slight injury, 1–6; moderate injury, 7–12; serious injury, 13–18). ICH rats with final scores of higher than 8 were included in subsequent experiments. Researchers were blinded to the experimental conditions and treatment groups.

2.5. Gait Analysis. The rat limb motor functions were tested with the TreadScan™ Gait System (Clever System Inc., USA) 7 days after treatment using a previously described procedure [9]. The rats ran on a treadmill at 8 cm/s for 20 s, the footprints were recorded at 100 frames/s. The videos were analyzed using TreadScan™ software to assess the gait performance. The parameters assessed in this study were the run speed, regularity index of normal step sequence, print area, stance, and swing time.

2.6. Positron-Emission Tomography. Positron-emission tomography (PET) imaging of rat brains was conducted using micro-PET/computed tomography (CT) (Siemens, Germany). The rats were not provided with food and water for the overnight period prior to PET scanning. Rats were then anesthetized with 2% pentobarbital sodium (2 μL/g) and injected with ^{18}F-fluorodeoxyglucose (^{18}F-FDG) synthesized by the Department of Nuclear Medicine, Affiliated Hospital of Southwest Medical University. Thirty minutes later, a PET scan of the head was performed, and the PET images of the rat brain were analyzed to measure the hemorrhagic foci volume and glucose uptake.

2.7. Brain Water Content. The brain water content, a surrogate measure for brain edema, was measured, as previously reported [11]. Briefly, animals were anesthetized and decapitated. The brains were quickly removed, and right hemispheres were weighed (wet weight). After drying for 24 hr at 100°C, the hemispheres were weighed again (dry weight). The brain water content (%) was calculated using the following formula: (wet weight − dry weight)/wet weight × 100%.

2.8. Enzyme-Linked Immunosorbent Assay (ELISA). After anesthesia, blood was collected for serum preparation. ELISA kits were used to detect serum myelin basic protein (MBP) (Novus Biologicals), tumor necrosis factor-α (TNF-α) (Boster), neuron-specific enolase (NSE), and S100 calcium-binding protein b (S100B) concentrations (Nanjing Jiancheng Corp.) according to the manufacturer's instructions.

2.9. Pathologic Examination. Rats were perfused transcardially with 0.9% ice-cold normal saline (NS) followed by 4% paraformaldehyde (PFA) under deep anesthetization with an overdose anesthetic drug. The rat brains were removed and subjected to postfixation, concentration gradient dehydration, and snap freezing. The brains were then cut into 7 μm thick coronal sections using a frozen slicer (Leica, Germany). After staining with hematoxylin and eosin (H&E), samples were observed under an optical microscope (Olympus, Japan).

2.10. Immunohistochemistry Staining. The frozen sections were treated with 0.3% tritonX-100 in 0.01 M phosphate-buffered saline (PBS) and 3% hydrogen peroxide (H_2O_2) for permeabilization and to block endogenous peroxidase activity, respectively. They were then incubated with 10% goat serum for 20 min at room temperature to block any nonspecific staining. The sections were incubated with rabbit anti-galactocerebrosidase (GALC) (1 : 100, Invitrogen), clusters of differentiation 68 (CD68) (1 : 200, CST), arginase-1 (Arg-1) (1 : 100, CST), inducible nitric oxide synthase (iNOS) (1 : 00, CST), N-methyl D-aspartate acid receptor subunit 2A (NR2A) (1 : 200, CST), glutamate receptor-2 (Glu2R) (1 : 100, Boster), aquaporin-4 (AQP4) (1 : 100, Bioworld), mouse antimicrotubule-associated protein 2 (MAP2) (1 : 200, Santa Cruz), glial fibrillary acidic protein (GFAP) (1 : 200, Santa Cruz), aquaporin-9 (AQP9) (1 : 100, Santa Cruz), B-cell lymphoma-2 (Bcl-2) (1 : 200, Santa Cruz), Bcl-2-associated x (Bax) (1 : 200, Santa Cruz), and glutamine (Glu) (1 : 200, Abcam) at 4°C overnight. Sections were then rinsed before further incubation with corresponding biotinylated secondary antibodies (Invitrogen) at 37°C for 30 min. Then, following treatment with streptavidin–biotin complex (SABC) at 37°C for 30 min, the sections were colored with diaminobenzidine (DAB), and target proteins were labeled. Finally, sections were stained with hematoxylin at room temperature for 3 min to detect the nuclei, and images were obtained using a microscope (Olympus, Japan).

2.11. Terminal Deoxynucleotidyl Transferase-Mediated (dUTP) Nick End Labeling (TUNEL) Assay. According to the standard procedure for TUNEL (Roche), frozen brain sections were washed three times in PBS and then incubated with a solution of proteinase k at 37°C for 15 min. After washing twice with PBS, the sections were treated with TUNEL reaction mixture, a red fluorescein-labeled TUTP solution containing 10% terminal deoxynucleotidyl transferase (TdT) at 37°C for 1 hr in the dark. The nuclei were counterstained with 4,6-diamidino-2-phenylin-dole (DAPI) at room temperature for 5 min. The number of TUNEL-positive cells was quantified by selecting five microscopic fields from each section.

2.12. Western Blot. The total protein content was extracted from the right striatum and was estimated with the BCA protein assay kit (Beyotime). Equal amounts of sample proteins were separated using sodium dodecyl sulfate-polyacrylamide gel electrophoresis (SDS-PAGE) and then transferred onto a polyvinylidene difluoride membrane. After blocking with 5% nonfat milk, the membrane was incubated overnight with the primary antibodies (AQP4, AQP9, Bax, Bcl-2, iNOS, Arg-1, and β-actin) at 4°C, with β-actin acting as a control. The next day, further incubation with appropriate horseradish peroxidase (HRP)-conjugated secondary antibodies (Invitrogen) at room temperature for 2 hr. Blots were then read by a chemiluminescence system

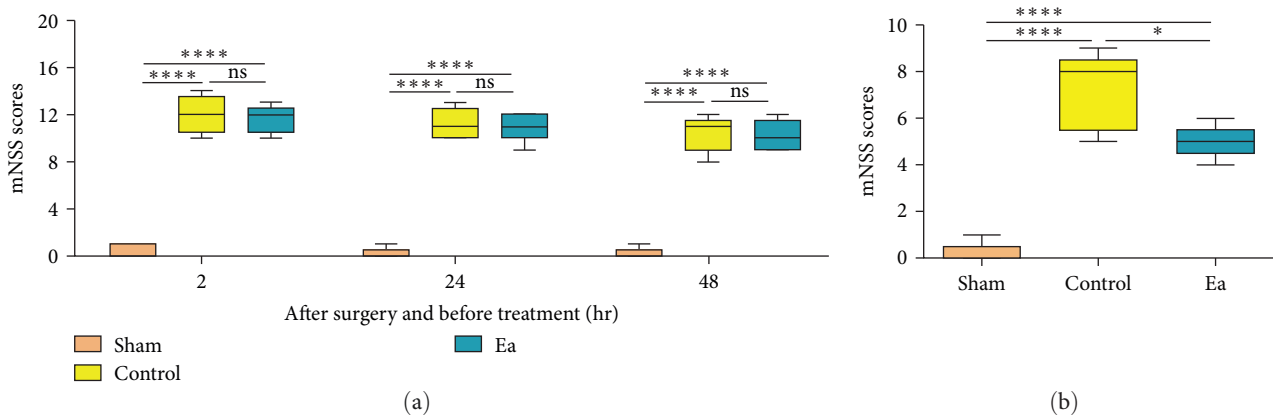

FIGURE 2: Neurological function tested with mNSS. (a) mNSS testing after ICH surgery but before treatment at different timepoints. (b) mNSS testing after treatment in different groups. $^{*}P<0.05$ and $^{****}P<0.0001$.

(Syngene G:BOX, UK) and quantification was performed with Quantity One software.

2.13. Statistical Analysis. All data were analyzed with GraphPad Prism 8.1 software and are presented as the mean ± standard deviation. Statistical significance was determined using the one-way analysis of variance test, and $P<0.05$ was considered statistically significant.

3. Results

3.1. Ea Reduced Neurological Symptoms. After ICH, the rats showed obvious neurobehavioral dysfunction. The mNSS scores in the Control and Ea groups were similar before treatment, but significantly higher than those in the Sham group (Figure 2(a)). After Ea treatment for 1 week, the Ea group showed significantly lower scores than the Control group ($P<0.05$, Figure 2(b)).

The footprints and strides of rats also changed significantly after ICH (Figures 3(a) and 3(b)). The gait analysis revealed that the run speed, regularity index of normal step sequence, and print area (rear left paw (RL)/rear right paw (RR)) decreased, while the stance time (RL) and swing time (RL) increased after ICH ($P<0.05$, Figure 3(c)–3(p)). However, Ea treatment was associated with significant increases in the run speed, regularity index of normal step sequence, print area (RL/RR), and stance time (RR) and decreases in the stance time (RL) and swing time (RL) in ICH rats ($P<0.05$, Figure 3(c)–3(p)).

3.2. Ea Reduced Hemorrhagic Foci. An ^{18}F-FDG micro-PET scan showed that the hemorrhagic area volumes were significantly smaller in the Ea compared with the Control group ($P<0.05$, Figures 4(a) and 4(b)). Moreover, there was no significant difference in the level of glucose uptake (ipsilateral/contralateral) between the Control and Ea groups (Figure 4(c)).

3.3. Ea Improved the Brain Tissue Structure. Figure 5(a) shows that the Contol and Ea groups developed prominent hemorrhagic foci after collagenase I and heparin injection, while no hemorrhagic focus was found in the Sham group, as expected. The Ea group presented significantly better brain tissue structure and smaller hematoma areas than the Control group ($P<0.05$, Figures 5(a) and 5(b)). H&E staining showed significantly larger lesion areas and an increased red blood cell (RBC) number in the Control group compared with the Ea group ($P<0.05$, Figures 5(c) and 5(d)).

3.4. Ea Regulated AQPs and Alleviated Cerebral Edema. The brain water content was significantly higher in the Control group compared with the Sham group, but lower in the Ea group compared with the Control group ($P<0.05$, Figure 6(a)). Furthermore, the expression levels of AQP4 and AQP9, which are also closely related to the brain water content, reduced significantly following Ea treatment ($P<0.05$, Figure 6(b)–6(h)).

3.5. Ea Alleviated Brain Injury. We tested the degree of brain damage by immunohistochemistry staining and ELISA. The data revealed that the MAP2 (a neuronal marker) and GALC (an oligodendrocyte marker) proteins increased significantly, but the number of GFAP (an astrocyte marker) positive cells decreased obviously in the Ea group compared with the Control group ($P<0.05$, Figure 7(a)–7(f)). Furthermore, the serum of NSE (a neuronal marker), MBP (an oligodendrocyte marker), and S100B (a marker of astrocyte activation and brain dysfunction) concentrations decreased significantly in the Ea group compared with the Control group ($P<0.05$, Figure (7(g)–7(i)).

3.6. Ea Reduced Cell Apoptosis and Regulated the Expression of Apoptosis-Related Proteins. The number of TUNEL-positive cells surrounding the hematoma significantly increased in the Control and Ea groups compared with the Sham group but decreased in the Ea group compared with the Control group ($P<0.05$, Figures 8(a) and 8(b)). The immunohistochemistry and western blotting analyses revealed that the Bcl-2 (an antiapoptotic marker) protein decreased; however, the Bax (a proapoptotic marker) protein increased after ICH ($P<0.05$, Figure 8(c)–8(i)). Bcl-2 expression increased and Bax expression decreased significantly in the Ea group compared with the Control group ($P<0.05$, Figure 8(c)–8(i)).

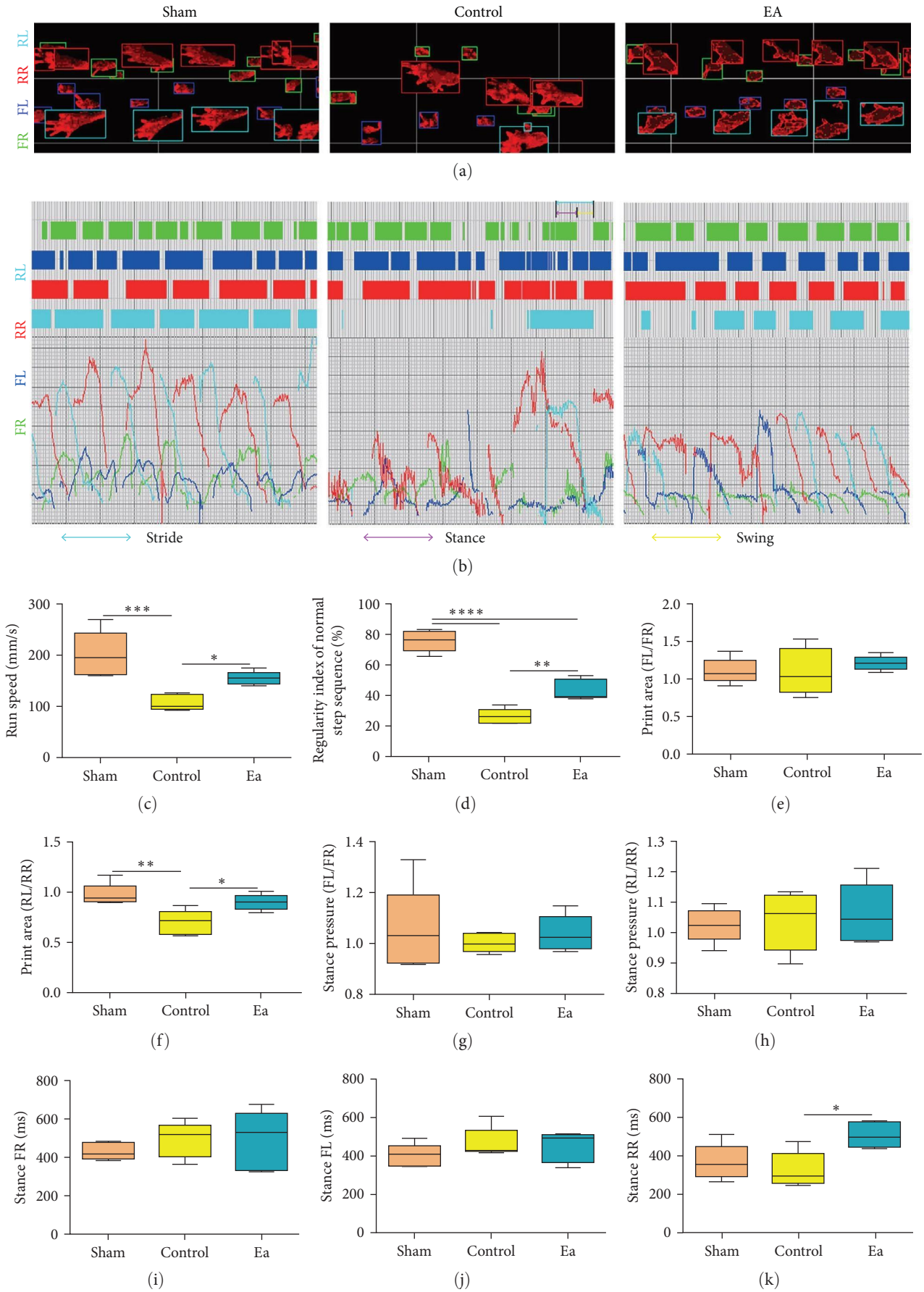

Figure 3: Continued.

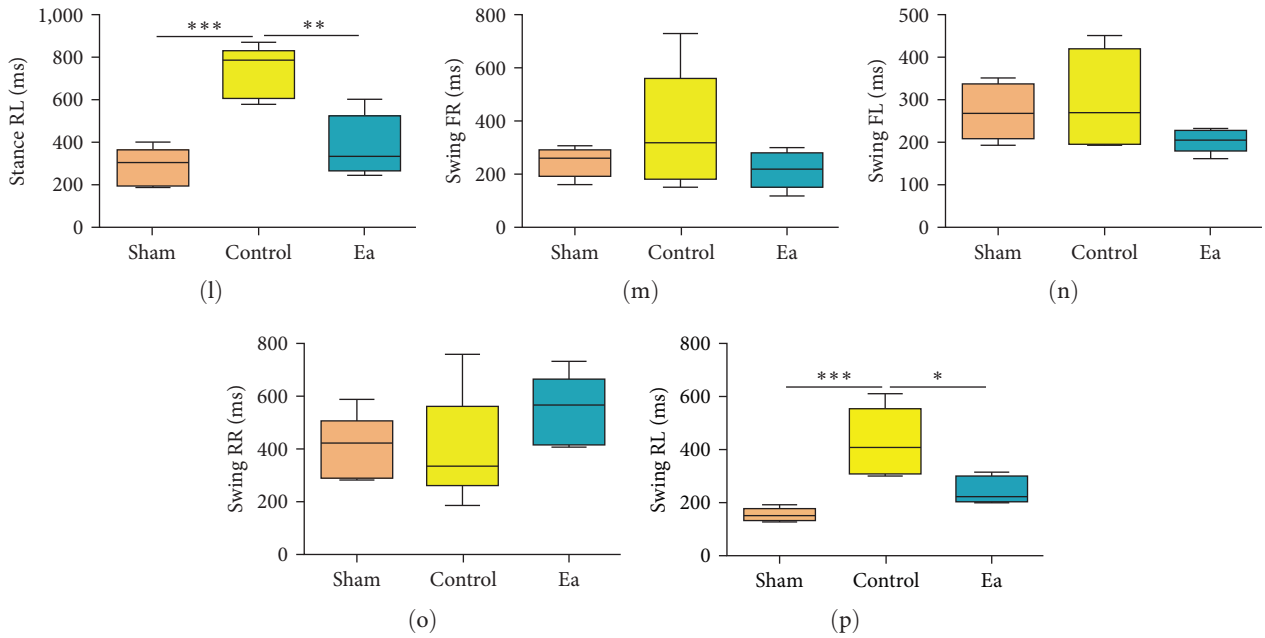

Figure 3: Gait analyzed using TreadScan. (a) Representative paw prints in different groups. The green, dark blue, red, and sky blue frames represent the front right (FR), front left (FL), rear right (RR), and rear left (RL) paw prints, respectively. (b) Representative strides in different groups. The green, dark blue, red, and sky blue frames represent the FR, FL, RR, and RL strides, respectively. (c–p) The gait analysis revealed the limb functions of rats from different groups. The gait parameters (including run speed, regularity index of normal step sequence, ratio of the print area, ratio of the stance pressure, stance, and swing) of the rats were analyzed using GAIT SCAN analysis software. $^{*}P<0.05$, $^{**}P<0.01$, $^{***}P<0.001$, and $^{****}P<0.0001$.

3.7. Ea Attenuated Excitotoxicity. Glu (a neurotransmitter) expression around hematomas was significantly upregulated following ICH-induced injury, but Ea treatment was associated with the downregulation of Glu expression ($P<0.05$, Figures 9(a) and 9(d)). Moreover, the expression of NR2A (a subunit of N-methyl-D-aspartic acid (NMDA) receptor) exhibited the same trend ($P<0.05$, Figures 9(b) and 9(e)). The Glu2R (a subunit of amino-3-hydroxy-5- methylisoxazole- 4-propionic acid (AMPA) receptor) level increased in the Ea group compared with the Control group ($P<0.05$, Figures 9(c) and 9(f)).

3.8. Ea Alleviated the Inflammatory Reaction. The number of cells positive for CD68 (a macrophage antigen marker) around the hematomas increased significantly in the Control and Ea groups compared with the Sham group. However, the number of CD68-positive cells decreased significantly in the Ea group compared with the Control group ($P<0.05$, Figure 10(a) and 10(b)).

The iNOS (M1 marker) and Arg-1 (M2 marker) positive cells significantly increased after ICH ($P<0.05$, Figure 10(c)–10(f)). The number of iNOS-positive cells was significantly lower in the Ea group than in the Control group ($P<0.05$, Figure 10(e)). However, the number of Arg-1 positive cells was higher in the Ea groups than in the Control group ($P<0.05$, Figure 10(f)). Western blot results revealed that Ea treatment upregulated the Arg-1 protein but downregulated the iNOS protein in rats subjected to ICH ($P<0.05$, Figure 10(g)–10(i)).

In comparison with the Sham group, serum TNF-α concentrations increased significantly in the Control and Ea groups ($P<0.05$), while serum TNF-α concentrations decreased obviously in the Ea group compared with the Control group ($P<0.05$, Figure 10(j)).

4. Discussion

In this study, we used mNSS and the TreadScan Gait System to assess the effects of Ea on neurological function in an ICH rat model. We found significant differences between the Control and Ea groups in terms of mNSS scores and some gait parameters such as the run speed and regularity index of normal step sequence. The results reveal that Ea administration could significantly improve neurological function in ICH rats.

By using ^{18}F-FDG micro-PET scanning to detect the bleeding area [9–11], the results showed that Ea treatment reduced the hemorrhagic focal area. This is significant as the extent of a brain injury is closely associated with brain edema and the duration of edema [12, 13]. Our results showed that the brain water content increased in rats by Day 7 after ICH and that Ea therapy was associated with brain edema alleviation. Aquaporins (AQPs), a family of water-channel proteins, play critical roles in homeostasis and water movement [14, 15]. Some studies have shown that AQP4 and AQP9 are associated with brain edema induced by several types of brain damage, including ICH, brain trauma, and ischemic stroke [16–18]. However, the effect of Ea on AQPs expression in the brain after ICH remains unclear. Our experimental study showed that the expression levels of the AQP4 and AQP9 proteins were lower in the Ea groups than in the

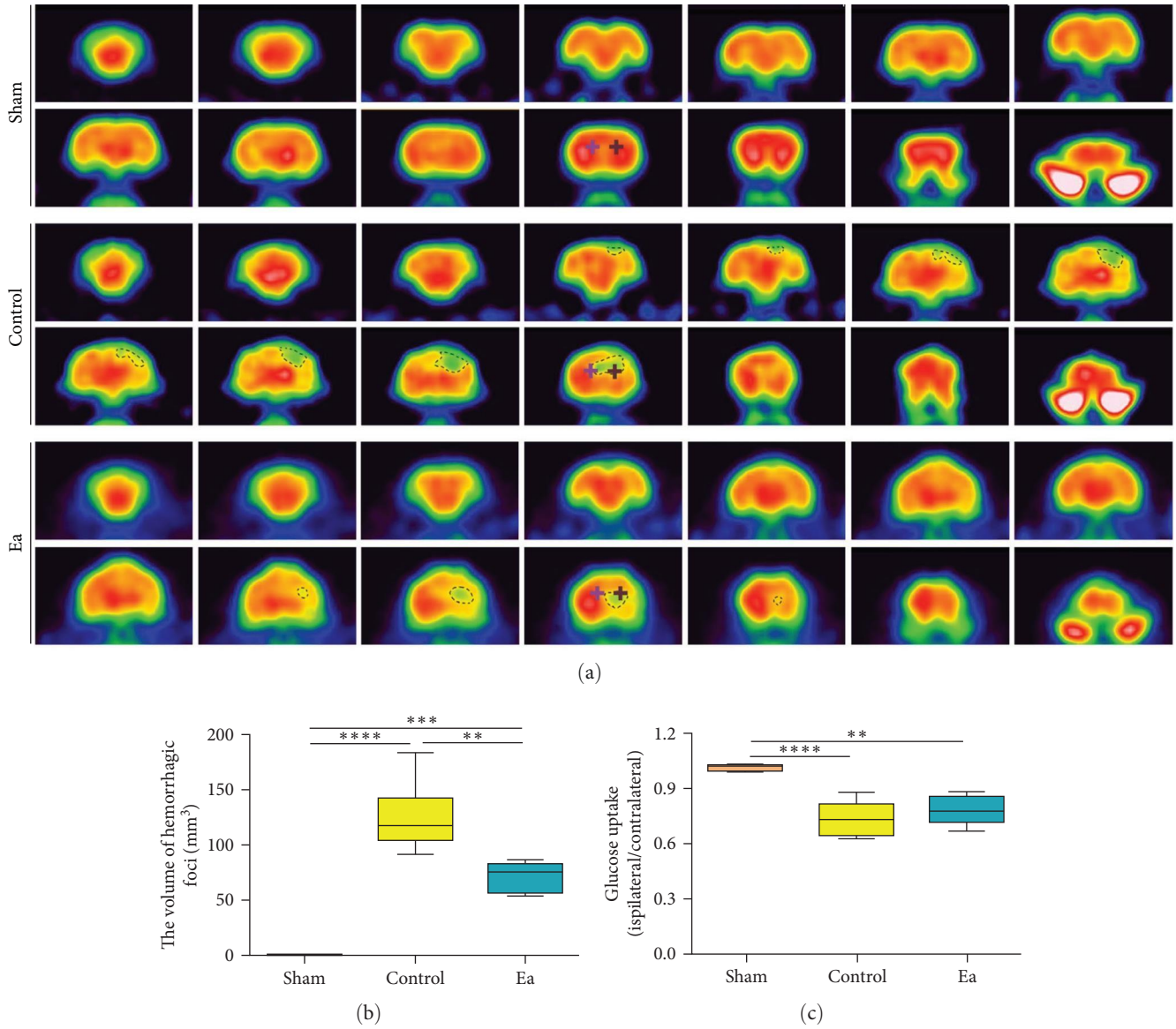

Figure 4: The hemorrhagic foci and glucose uptake detected using ^{18}F-FDG PET. (a) PET axial images of the rat brains from different groups. The dotted area represents the hemorrhagic focus, and the two pluses represent the contralateral and ipsilateral checkpoints of glucose uptake. (b) Statistical analysis of the volume of the hemorrhage foci in rats from different groups via ^{18}F-FDG micro-PET scan. (c) The glucose uptake (ipsilateral/contralateral) in different groups was determined via ^{18}F-FDG micro-PET scan. $^{**}P<0.01$, $^{***}P<0.001$, and $^{****}P<0.0001$.

Control group, suggesting that Ea may reduce brain edema by regulating the AQP4 and AQP9 proteins.

ICH can lead to significant cell death through a variety of mechanisms, including those involving neurons and glial cells [19–21]. The death of oligodendrocytes and neurons has been associated with demyelination and neurological dysfunction [19, 22]. Previous studies have shown that Ea improves neurobehavioral function and brain injury in ICH rats [9]. In the present study, Ea stimulation increased MAP2 and GALC expression and decreased GFAP expression, implying that Ea promotes the survival of neurons and oligodendrocytes and inhibits astrocyte hyperplasia in rats subjected to ICH. In addition, serum concentrations of the MBP, NSE, and S100B proteins, common indicators of the severity of hemorrhagic brain injury [23, 24], are often used as diagnostic and prognostic biomarkers for brain injury [25–27]. We found that Ea treatment downregulated these proteins in the serum, indicating that Ea treatment relieved brain injury in rats after ICH.

A growing body of evidence suggests that cell apoptosis plays an important role in the pathogenesis of ICH-induced brain injury [28, 29]. The Bcl-2 and Bax proteins play vital roles in regulating apoptosis [30, 31]. Previously, Ea treatment has been shown to inhibit cell apoptosis, thereby inducing neuroprotection against ischemic injury [32]. In order to investigate whether the regulation of apoptosis by Ea (GV20-GV14) could play a neuroprotective role against ICH, the effects of Ea on cell apoptosis and apoptosis-related

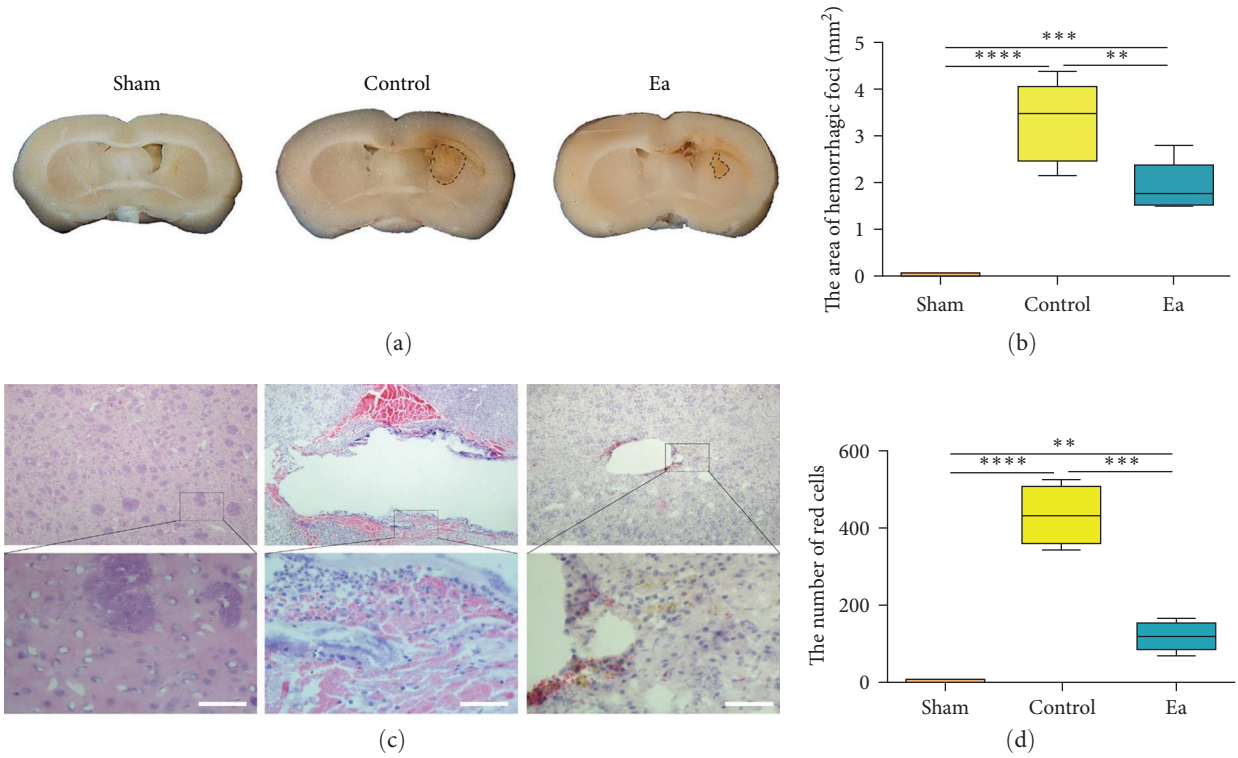

Figure 5: The effects of Ea on the brain tissue structure. (a) The coronal sections of the brains show hemorrhagic foci in rats with ICH. (b) The area of hemorrhagic foci on the coronal sections of the brains. (c) Histological features of rat brains (H&E staining). (d) The number of RBCs in the coronal sections of the brains. $^{**}P<0.01$, $^{***}P<0.001$, and $^{****}P<0.0001$. Bar = 100 μm.

proteins were evaluated. The results showed that Ea treatment may inhibit ICH-induced apoptosis by upregulating Bcl-2 and decreasing Bax expression.

Glu, the most abundant neurotransmitter in the CNS, is not restricted to synaptic clefts but exists in the extrasynaptic regions as ambient glutamate [33]. Previous studies using ICH models have investigated the relationship between brain injury and Glu levels in perihematomal brain tissues, the impact of the Glu level on outcomes in ICH patients, and the challenges posed by Glu excitotoxicity in the management of hemorrhagic stroke [34–36]. In a rabbit model of ICH, minimally invasive removal of intracerebral hematoma was found to decrease perihematomal glutamate level and neurological deficit score [37]. In addition, a clinical study found that the Glu level was increased in the perihematomal region after ICH and decreased during hematoma drainage [34]. The NMDA receptor (NR) is an ionotropic glutamate receptor composed of NR1, NR2A-D, and NR3 subunits that play critical roles in the physiological and pathological processes of the CNS [38]. The fragmentation of the NR2 subunit into NR2A and NR2B peptides may be caused by stroke or neurotoxicity; thus, the NR peptide is an indicator of Glu excitotoxicity associated with stroke pathophysiology [39]. GluR2 plays an important role in the prevention and cure of brain injury, largely by reducing the permeability of the AMPA receptors (AMPARs) to Ca^{2+} [40]. A decrease in GluR2 subunits may cause an influx of Ca^{2+}, which may be involved in cortical neuron neurotoxicity [41]. In this study, we found that ICH increased the expression of Glu, NR2A, and GluR2, but Ea decreased the expression of Glu and NR2A, and further improved the expression of GluR2. We speculate that Ea depresses the Ca^{2+}-permeability of AMPARs with GluR2 subunits and alleviates the effect of excitotoxicity mediated by Glu and NR2A in ICH rat brains.

Numerous studies have demonstrated the important role of inflammation characterized by microglia/macrophage activation in hemorrhagic brain injury [42–44]. Microglia in the CNS milieu can be categorized into two opposite types, proinflammatory M1 phenotype and anti-inflammatory M2 phenotype, which produce cytotoxic and neuroprotective effects, respectively. Activation of the microglia after ICH exacerbates the production of proinflammatory factors, such as TNF-α and iNOS. Therefore, anti-inflammatory methods may alleviate brain injury and improve neurological functions after ICH [45]. Several studies have reported that Ea significantly induced anti-inflammatory responses in obese and ischemic stroke patients, as well as in individuals with infectious and inflammatory disorders [46–48]. Our data show that Ea significantly inhibited microglia activation, downregulated TNF-α, CD68, and iNOS expression, and upregulated Arg-1 expression in rats after ICH. Ea also exerted an anti-inflammatory effect on ICH rats.

There are mutual influences and connections between brain edema, inflammation, and excitatory toxicity caused by ICH. After collagenase-induced ICH, the brain water content increased on Day 1, reached a peak on Day 3, and was still higher than that in the sham group on Day 10 [49]; Microglia are activated as early as 1 hr post-ICH. The

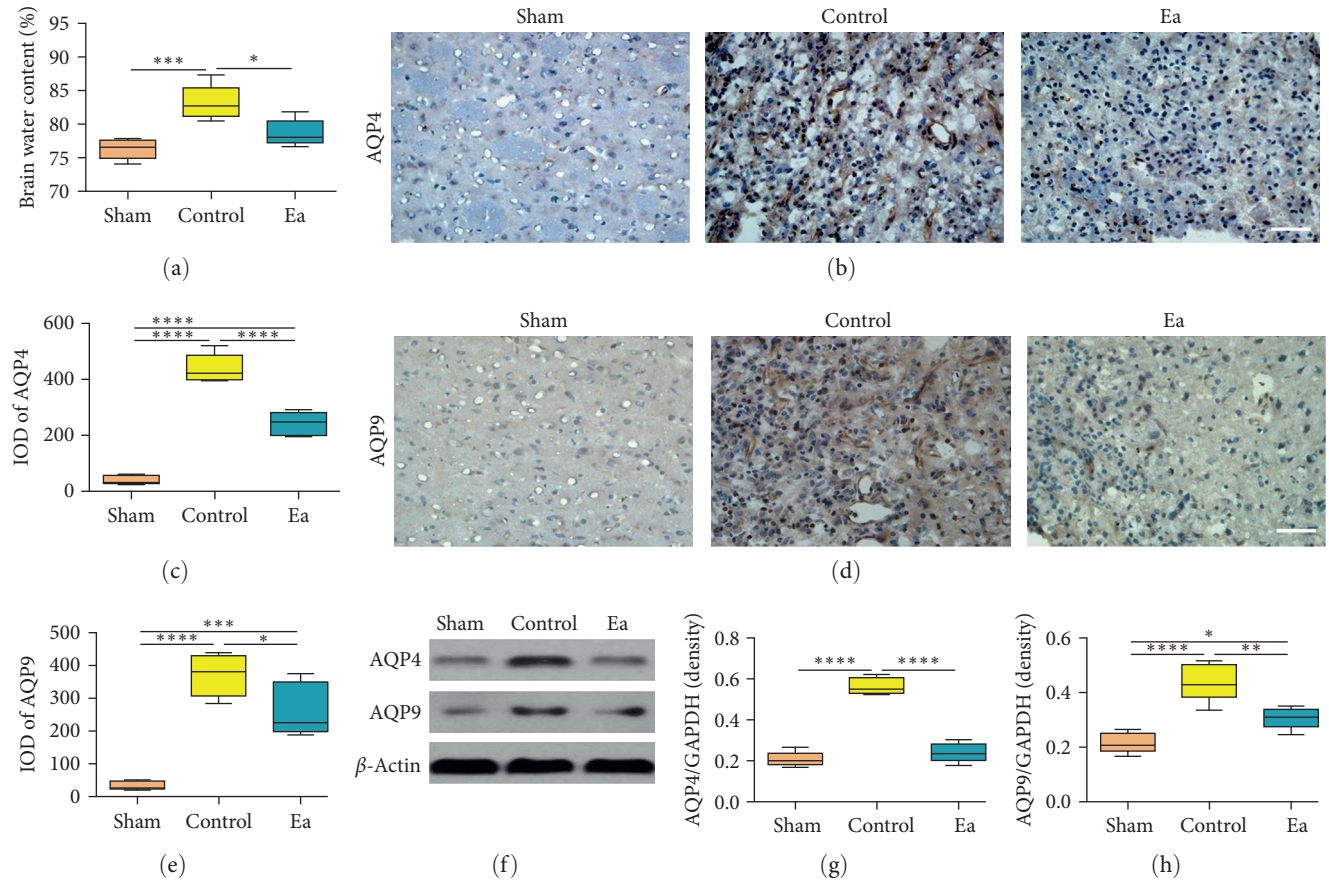

Figure 6: The effects of Ea on mNSS, brain edema, and expressions of AQP4 and AQP9 proteins in rats after ICH. (a) The brain water content of rats from different groups. Representative images of AQP4 (b) and AQP9 (d) immunohistochemical staining in the rat ipsilateral striatum. Statistical analyses of AQP4 (c) and AQP9 (e) immunopositive staining. Representative results (f) and quantitative analyses (g, h) of western blot showing the relative expression levels of the AQP4 and AQP9 proteins in the rat ipsilateral striatum. $^{*}P<0.05$, $^{**}P<0.01$, $^{***}P<0.001$, and $^{****}P<0.0001$. Bar = 100 μm.

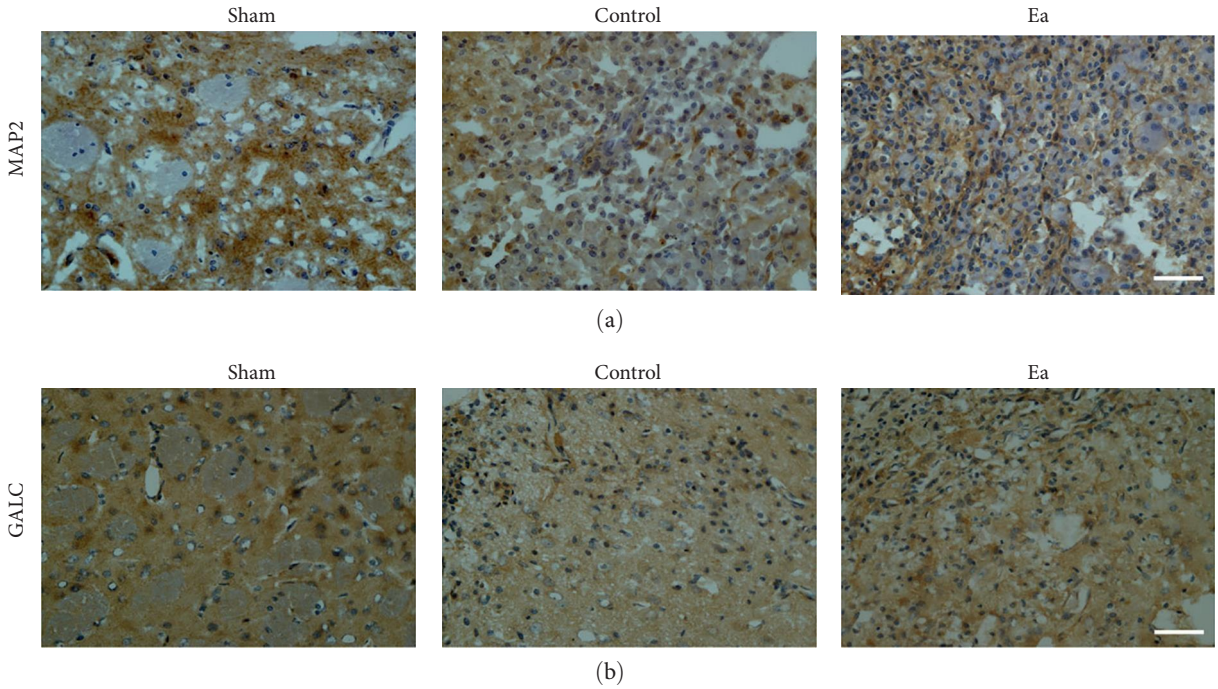

Figure 7: Continued.

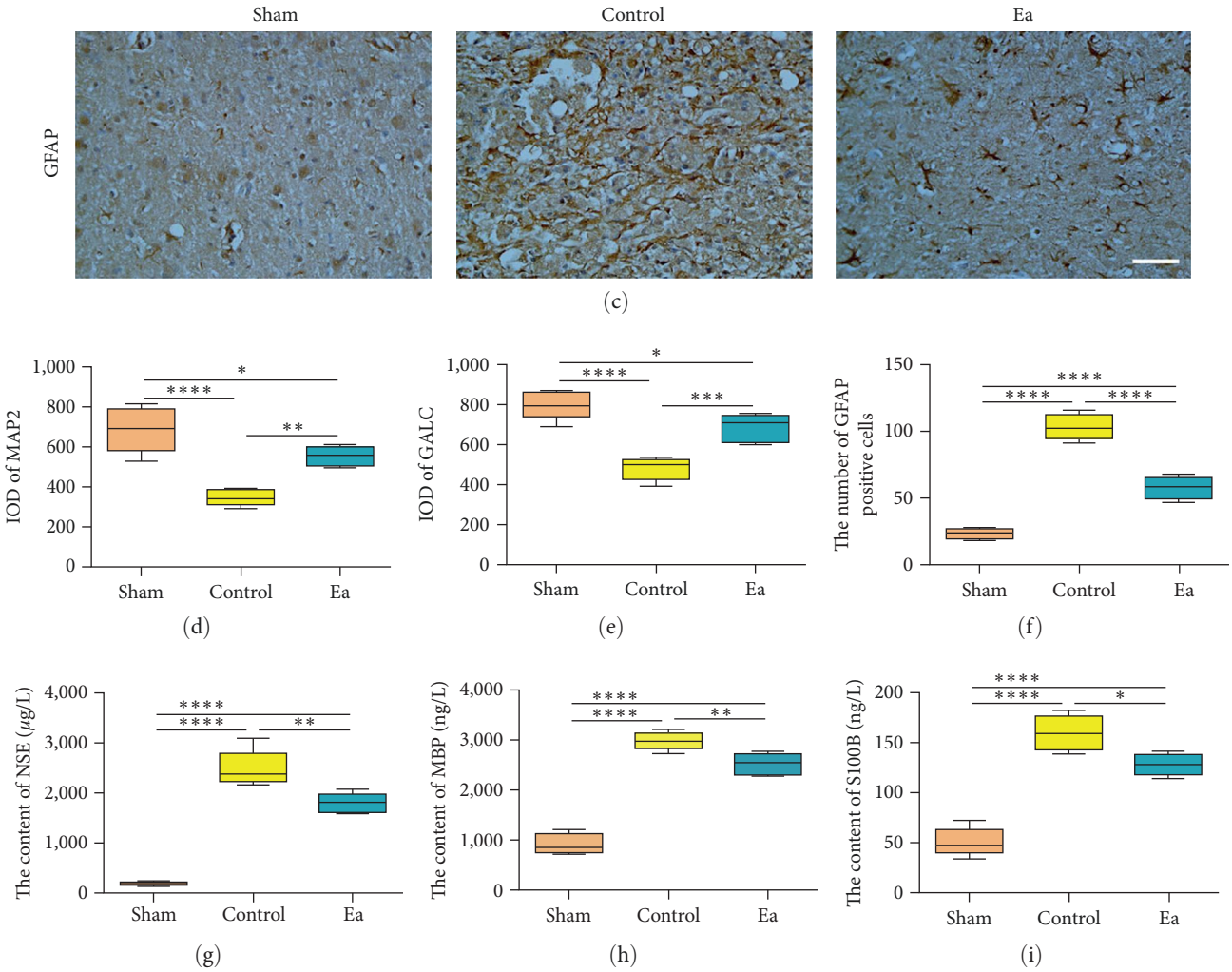

Figure 7: The effects of Ea on the expression levels of MAP2, GALC, and GFAP proteins in the brain, and the contents of NSE, MBP, and S100B in rat serum. Representative images of MAP2 (a), GALC (b), and GFAP (c) immunohistochemical staining in the rat ipsilateral striatum. Statistical analyses of MAP2 (d), GALC (e), and GFAP (f) immunopositive staining. Quantitative analyses of ELISA showing the serum levels of the NSE (g), MBP (h), and S100B (i) proteins. $^{*}P<0.05$, $^{**}P<0.01$, $^{***}P<0.001$, and $^{****}P<0.0001$. Bar = 100 μm.

number of activated microglia/macrophages then peaks at 72 hr and gradually returns to normal levels, which takes several weeks [50]. ICH causes the release of many endogenous molecules, including heme, glutamate, TNF-α, and reactive oxygen species. These molecules are involved in mitotic signaling transduction and excitatory toxicity. Mitotic signaling initiates the cell cycle to produce the normal division of neural stem cells and microglia, whereas aberrant mitotic signaling may lead to excitatory toxicity [51]. After ICH, IL-10 defective mice have been found to present more serious brain edema, inflammation, and neurological deficits related to delayed hematoma clearance [52]. On the one hand, insufficient RBC clearance by activated microglia may prolong injury and worsen outcomes. On the other hand, overactive microglia may lead to secondary damage [52, 53]. Microglia respond to ICH by becoming activated and developing into a classic M1 phenotype or an alternative M2 phenotype. Microglial polarization affects both the pathological process and recovery post-ICH, and this may be associated with the production of proinflammatory or anti-inflammatory cytokines and chemokines [54–56]. Moreover, M2 phenotype microglia can promote the phagocytosis of RBCs and tissue debris, which is the main contributor to hematoma clearance [54].

Several limitations of this study need to be mentioned. First, Ea plays a variety of roles in tissue repair and neurological rehabilitation. Although we observed the effects of Ea on the brain water content and aquaporins, the underlying mechanisms need to be further investigated. Second, our immunohistochemistry and western blot experiments show that Ea promoted the transformation of microglia from the M1 type to the M2 type after ICH, but further research on its signal regulation is required. In addition, we only observed the brain water content and microglial polarization during

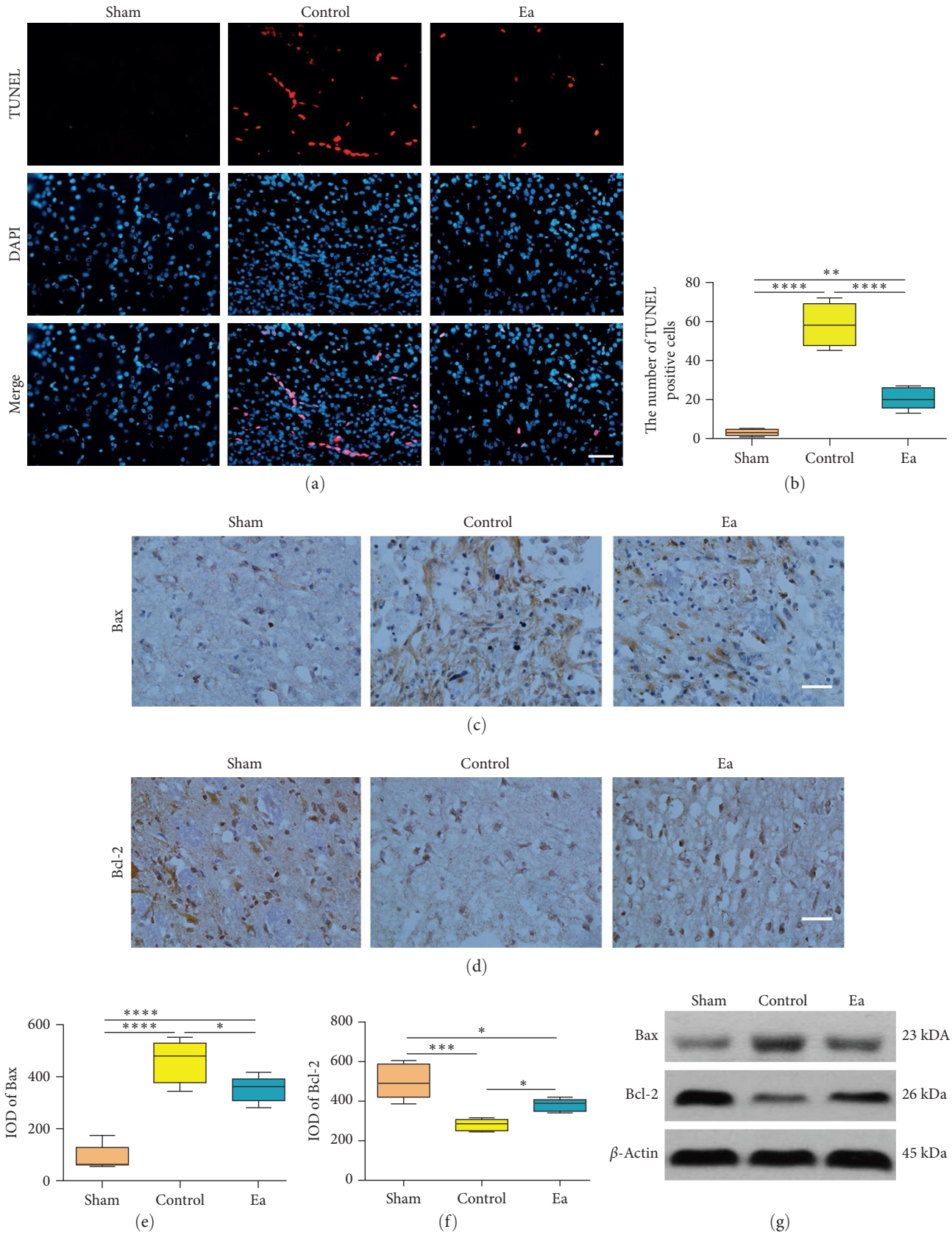

Figure 8: Continued.

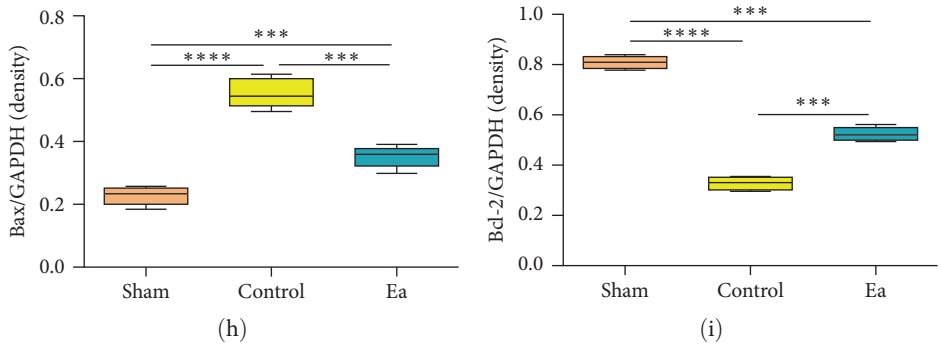

Figure 8: The effects of Ea on cell apoptosis and the expression of apoptosis-related proteins. (a) Representative images of TUNEL staining in the rat ipsilateral striatum. (b) Quantitative analysis of TUNEL-positive cells in each group. Representative images of Bax (c) and Bcl-2 (d) immunohistochemical staining in the ipsilateral striatum of the rats. Statistical analyses of Bax (e) and Bcl-2 (f) immunopositive staining. Representative results (g) and quantitative analyses (h, i) of Western blot showing the relative expression of the Bax and Bcl-2 proteins in the rat ipsilateral striatum. $^{*}P<0.05$, $^{**}P<0.01$, $^{***}P<0.001$, and $^{****}P<0.0001$. Bar = 100 μm.

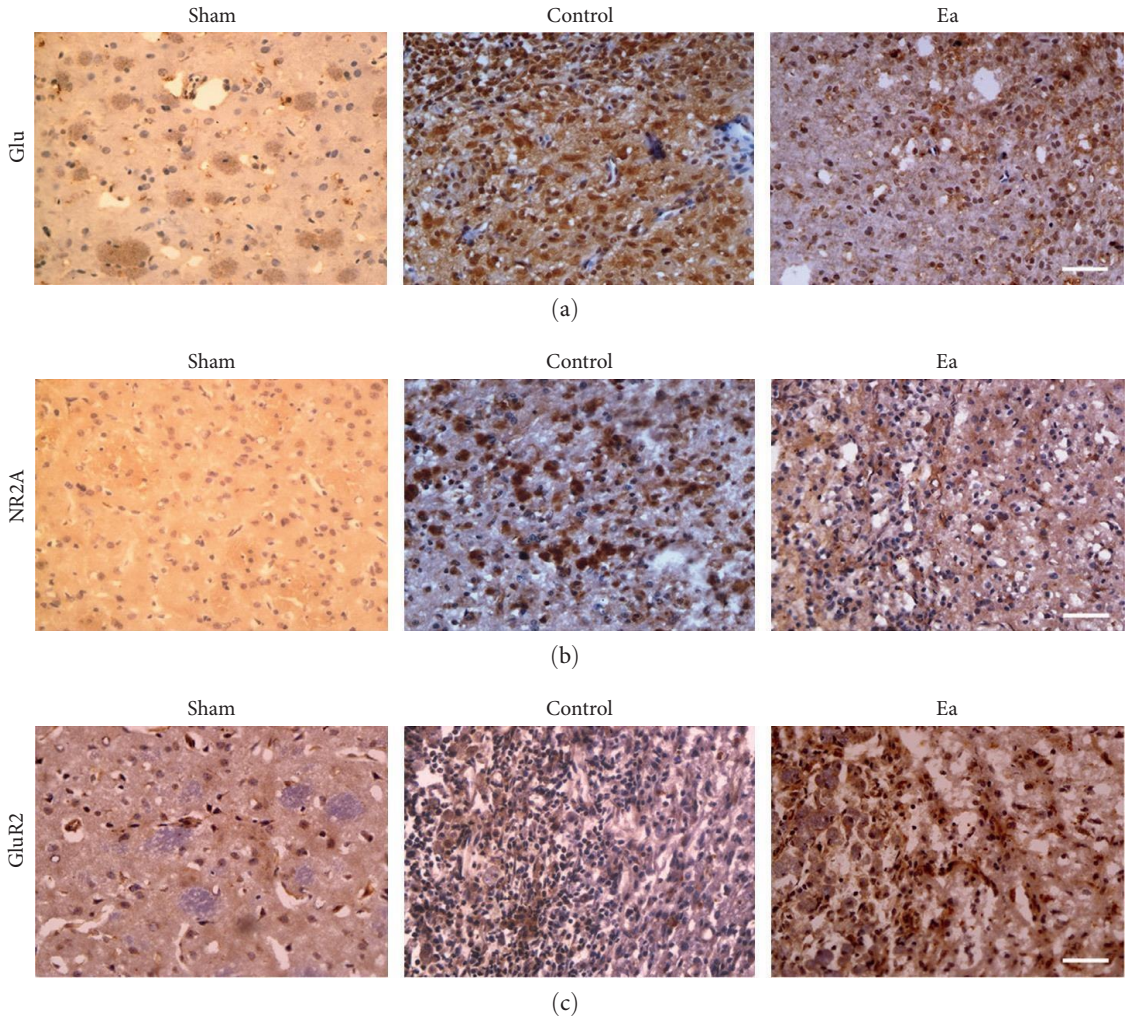

Figure 9: Continued.

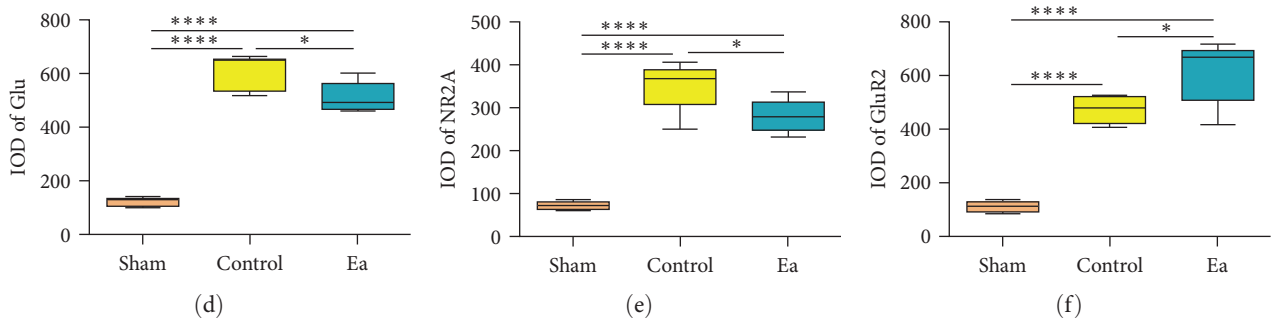

Figure 9: The effect of Ea on the levels of Glu, NR2A, and Glu2R proteins in the brain. Representative images of the Glu (a), NR2A (b), and Glu2R (c) immunohistochemical staining in rat ipsilateral striatum. Quantification analyses of Glu (d), NR2A (e), and Glu2R (f) immunohistochemical staining. $^{*}P<0.05$ and $^{****}P<0.0001$. Bar = 100 μm.

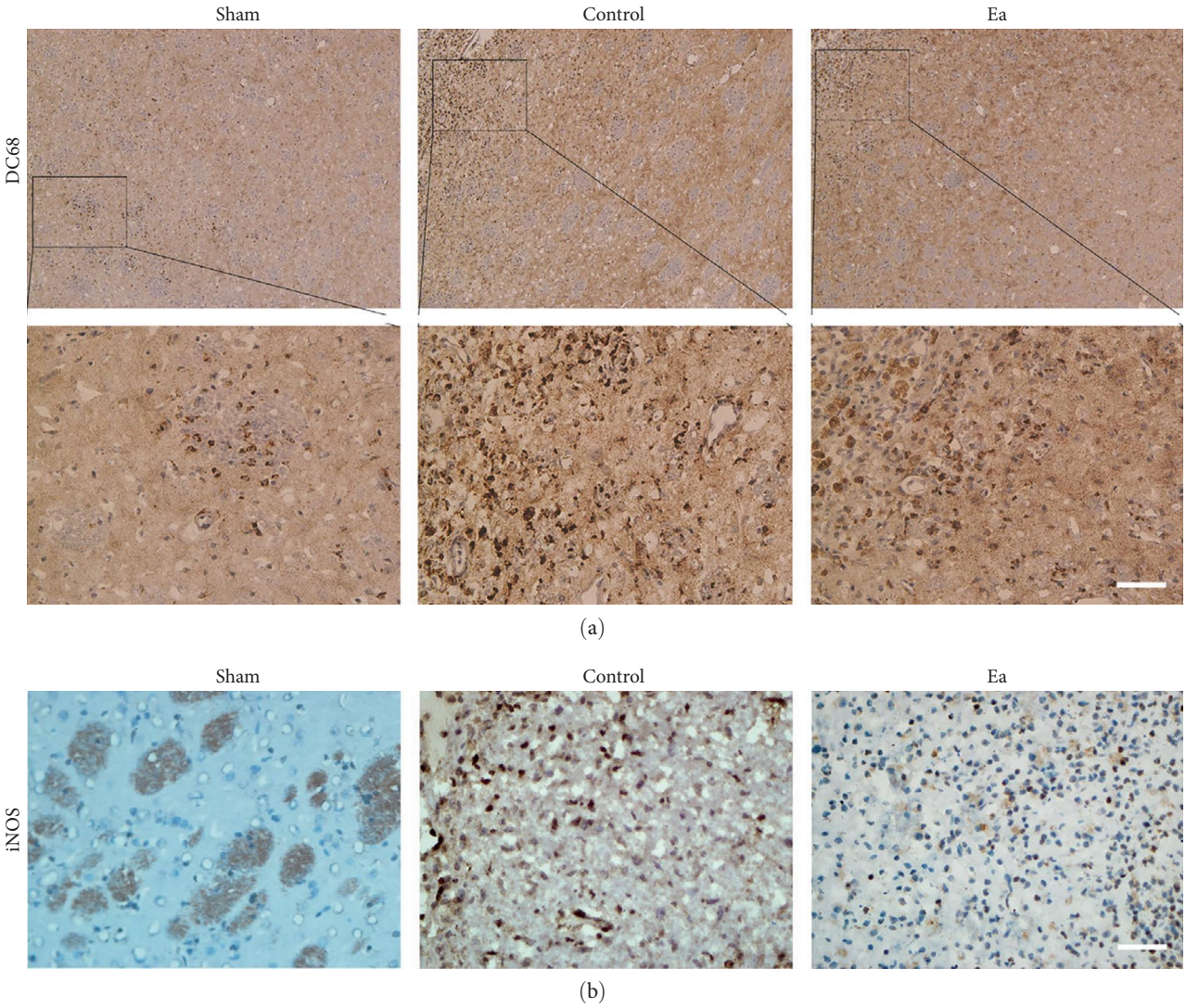

Figure 10: Continued.

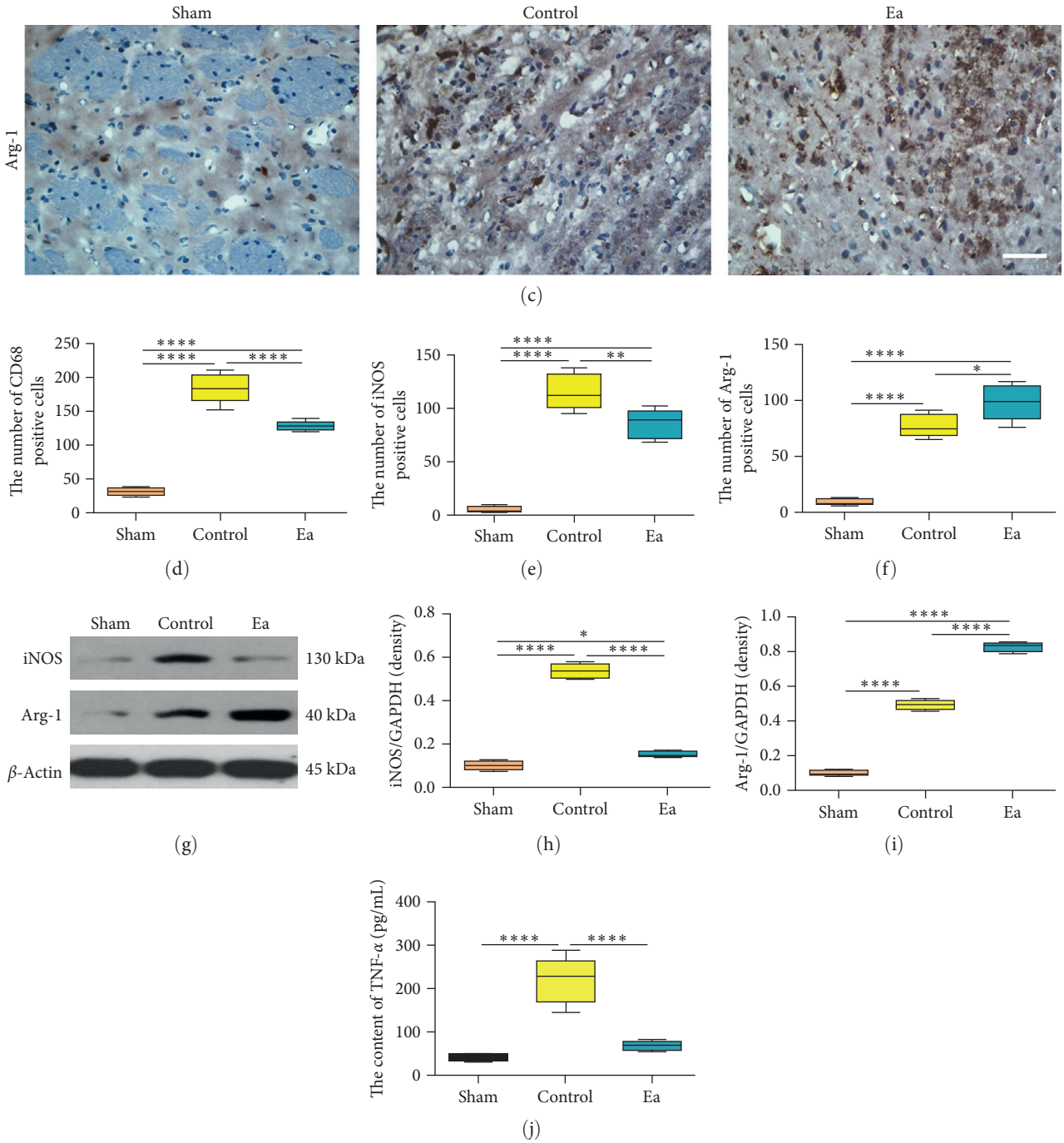

FIGURE 10: The effect of Ea on the inflammatory reaction. Representative images of CD68 (a), iNOS (b), and Arg-1 (c) immunohistochemistry in the rat ipsilateral striatum. Quantitative analysis of the CD68 (d), iNOS (e), and Arg-1(f) positive cells. Representative results (g) and quantitative analyses (h, i) of western blot showing the relative expression of the iNOS and Arg-1 proteins in the rat ipsilateral striatum. (j) ELISA results show the serum TNF-α concentration in different groups. $^{*}P<0.05$, $^{**}P<0.01$, and $^{****}P<0.0001$. Bar = 100 μm.

the first week of Ea treatment, while research on sustained changes in hematomas and the brain water content after microglial polarization is still lacking.

5. Conclusions

In short, although the present study has some limitations, we demonstrated that Ea treatment could effectively improve the symptoms of neurological deficits and reduce brain edema, apoptosis, and excitotoxicity in rats after ICH. We speculate that Ea plays an important role in inhibiting inflammatory responses. As a consequence of this neuroprotection, brain tissue functions may be restored. Further studies and an optimized experimental design are now warranted to better understand and investigate the mechanisms involved. Nevertheless, the results of the present study suggest that the

administration of Ea may be an important therapeutic strategy to alleviate hemorrhagic brain injury.

Data Availability

The data used to support the findings of this study are available from the corresponding authors upon reasonable request.

Ethical Approval

This study was carried out in accordance with the guidelines of the People's Republic of China on experimental animals. The animal experiment was submitted to and approved by the Ethical Committee for Animal Experimental Center of the Southwest Medical University.

Conflicts of Interest

The authors declare that they have no conflicts of interest.

Authors' Contributions

CY conceived and designed the experiments and revised the manuscript. LH, XF, YC, HL, and XJ performed the experiments and analyzed the data. LH and XF wrote the manuscript. All authors read and approved the final manuscript. Li Huang and Xuehui Fan contributed equally to this work.

Acknowledgments

This study was supported by the Research Project of Medical Electrophysiological Key Laboratory (KeyME-2022-05) and the Natural Science Foundation of Sichuan Province (2022NSFSC0718).

References

[1] GBD 2019 Stroke Collaborators, "Global, regional, and national burden of stroke and its risk factors, 1990–2019: a systematic analysis for the global burden of disease study 2019," *Lancet Neurology*, vol. 20, no. 10, pp. 795–820, 2021.

[2] M. Chen, J. Sun, C. Lu et al., "The impact of neuronal Notch-1/JNK pathway on intracerebral hemorrhage-induced neuronal injury of rat model," *Oncotarget*, vol. 7, no. 45, pp. 73903–73911, 2016.

[3] H.-Q. Li, Y. Li, Z.-X. Chen et al., "Electroacupuncture exerts neuroprotection through caveolin-1 mediated molecular pathway in intracerebral hemorrhage of rats," *Neural Plasticity*, vol. 2016, Article ID 7308261, 8 pages, 2016.

[4] H.-J. Zhou, T. Tang, J.-H. Zhong et al., "Electroacupuncture improves recovery after hemorrhagic brain injury by inducing the expression of angiopoietin-1 and -2 in rats," *BMC Complementary and Alternative Medicine*, vol. 14, no. 1, Article ID 127, 2014.

[5] X.-H. Zhang, C.-C. Feng, L.-J. Pei et al., "Electroacupuncture attenuates neuropathic pain and comorbid negative behavior: the involvement of the dopamine system in the amygdala," *Frontiers in Neuroscience*, vol. 15, Article ID 657507, 2021.

[6] C. Inprasit and Y.-W. Lin, "TRPV1 responses in the cerebellum Lobules V, VIa and VII using electroacupuncture treatment for inflammatory hyperalgesia in murine model," *International Journal of Molecular Sciences*, vol. 21, no. 9, Article ID 3312, 2020.

[7] J. Li, L. Chen, D. Li et al., "Electroacupuncture promotes the survival of the grafted human MGE neural progenitors in rats with cerebral ischemia by promoting angiogenesis and inhibiting inflammation," *Neural Plasticity*, vol. 2021, Article ID 4894881, 11 pages, 2021.

[8] J. Zhao, L. Wang, and Y. Li, "Electroacupuncture alleviates the inflammatory response via effects on M1 and M2 macrophages after spinal cord injury," *Acupuncture in Medicine*, vol. 35, no. 3, pp. 224–230, 2017.

[9] Y. Zhu, L. Deng, H. Tang et al., "Electroacupuncture improves neurobehavioral function and brain injury in rat model of intracerebral hemorrhage," *Brain Research Bulletin*, vol. 131, pp. 123–132, 2017.

[10] L. Deng, L. Zhou, Y. Zhu et al., "Electroacupuncture enhance therapeutic efficacy of mesenchymal stem cells transplantation in rats with intracerebral hemorrhage," *Stem Cell Reviews and Reports*, vol. 18, no. 2, pp. 570–584, 2022.

[11] J. Zeng, Y. Chen, R. Ding et al., "Isoliquiritigenin alleviates early brain injury after experimental intracerebral hemorrhage via suppressing ROS- and/or NF-kappaB-mediated NLRP3 inflammasome activation by promoting Nrf2 antioxidant pathway," *Journal of Neuroinflammation*, vol. 14, no. 1, Article ID 119, 2017.

[12] X. Liu, G. Wu, N. Tang et al., "Glymphatic drainage blocking aggravates brain edema, neuroinflammation via modulating TNF-alpha, IL-10, and AQP4 after intracerebral hemorrhage in rats," *Frontiers in Cellular Neuroscience*, vol. 15, Article ID 784154, 2021.

[13] G. Yang, J. Zhu, G. Zhan et al., "Mesenchymal stem cell-derived neuron-like cell transplantation combined with electroacupuncture improves synaptic plasticity in rats with intracerebral hemorrhage via mTOR/p70S6K signaling," *Stem Cells International*, vol. 2022, Article ID 6450527, 13 pages, 2022.

[14] M. C. Papadopoulos and A. S. Verkman, "Aquaporin water channels in the nervous system," *Nature Reviews Neuroscience*, vol. 14, no. 4, pp. 265–277, 2013.

[15] K. Wagner, L. Unger, M. M. Salman, P. Kitchen, R. M. Bill, and A. J. Yool, "Signaling mechanisms and pharmacological modulators governing diverse aquaporin functions in human health and disease," *International Journal of Molecular Sciences*, vol. 23, no. 3, Article ID 1388, 2022.

[16] B.-F. Wang, Z.-W. Cui, Z.-H. Zhong et al., "Curcumin attenuates brain edema in mice with intracerebral hemorrhage through inhibition of AQP4 and AQP9 expression," *Acta Pharmacologica Sinica*, vol. 36, no. 8, pp. 939–948, 2015.

[17] H. Wu, C. Tang, L. W. Tai et al., "Flurbiprofen axetil attenuates cerebral ischemia/reperfusion injury by reducing inflammation in a rat model of transient global cerebral ischemia/reperfusion," *Bioscience Reports*, vol. 38, no. 4, 2018.

[18] J. Yin, H. Zhang, H. Chen, Q. Lv, and X. Jin, "Hypertonic saline alleviates brain edema after traumatic brain injury via downregulation of aquaporin 4 in rats," *Medical Science Monitor*, vol. 24, pp. 1863–1870, 2018.

[19] W. Chen, C. Guo, Z. Jia et al., "Inhibition of mitochondrial ROS by MitoQ alleviates white matter injury and improves outcomes after intracerebral haemorrhage in mice," *Oxidative Medicine and Cellular Longevity*, vol. 2020, Article ID 8285065, 12 pages, 2020.

[20] Y. Kong, S. Li, M. Zhang et al., "Acupuncture ameliorates neuronal cell death, inflammation, and ferroptosis and downregulated miR-23a-3p after intracerebral hemorrhage

in rats," *Journal of Molecular Neuroscience*, vol. 71, no. 9, pp. 1863–1875, 2021.

[21] W.-D. Bao, X.-T. Zhou, L.-T. Zhou et al., "Targeting miR-124/Ferroportin signaling ameliorated neuronal cell death through inhibiting apoptosis and ferroptosis in aged intracerebral hemorrhage murine model," *Aging Cell*, vol. 19, no. 11, Article ID e13235, 2020.

[22] J. Lu, Z. Li, Q. Zhao, D. Liu, and Y.-A. Mei, "Neuritin improves the neurological functional recovery after experimental intracerebral hemorrhage in mice," *Neurobiology of Disease*, vol. 156, Article ID 105407, 2021.

[23] E. Martínez-Morillo, P. G. Hernández, I. Begcevic et al., "Identification of novel biomarkers of brain damage in patients with hemorrhagic stroke by integrating bioinformatics and mass spectrometry-based proteomics," *Journal of Proteome Research*, vol. 13, no. 2, pp. 969–981, 2014.

[24] X. Li, X. Huang, Y. Tang et al., "Assessing the pharmacological and therapeutic efficacy of traditional Chinese medicine liangxue tongyu prescription for intracerebral hemorrhagic stroke in neurological disease models," *Frontiers in Pharmacology*, vol. 9, Article ID 1169, 2018.

[25] A. Kanavaki, K. Spengos, M. Moraki et al., "Serum levels of S100b and NSE proteins in patients with non-transfusion-dependent thalassemia as biomarkers of brain ischemia and cerebral vasculopathy," *International Journal of Molecular Sciences*, vol. 18, no. 12, Article ID 2724, 2017.

[26] Y. Li, W. Lv, G. Cheng et al., "Effect of early normobaric hyperoxia on blast-induced traumatic brain injury in rats," *Neurochemical Research*, vol. 45, no. 11, pp. 2723–2731, 2020.

[27] P. Katsanou, N. Tentolouris, D. Perrea et al., "S100B levels in patients with type 2 diabetes mellitus and co-occurring depressive symptoms," *Depression Research and Treatment*, vol. 2018, Article ID 5304759, 8 pages, 2018.

[28] Z. Wang, F. Zhou, Y. Dou et al., "Melatonin alleviates intracerebral hemorrhage-induced secondary brain injury in rats via suppressing apoptosis, inflammation, oxidative stress, DNA damage, and mitochondria injury," *Translational Stroke Research*, vol. 9, no. 1, pp. 74–91, 2018.

[29] T. Sugiyama, T. Imai, S. Nakamura et al., "A novel Nrf2 activator, RS9, attenuates secondary brain injury after intracerebral hemorrhage in sub-acute phase," *Brain Research*, vol. 1701, pp. 137–145, 2018.

[30] X.-K. Tu, Q. Chen, S. Chen, B. Huang, B.-G. Ren, and S.-S. Shi, "GLP-1R agonist liraglutide attenuates inflammatory reaction and neuronal apoptosis and reduces early brain injury after subarachnoid hemorrhage in rats," *Inflammation*, vol. 44, no. 1, pp. 397–406, 2021.

[31] Z. Li, G. Xiao, H. Wang, S. He, and Y. Zhu, "A preparation of *Ginkgo biloba* L. leaves extract inhibits the apoptosis of hippocampal neurons in post-stroke mice via regulating the expression of Bax/Bcl-2 and Caspase-3," *Journal of Ethnopharmacology*, vol. 280, Article ID 114481, 2021.

[32] S. Sun, X. Chen, Y. Gao et al., "Mn-SOD upregulation by electroacupuncture attenuates ischemic oxidative damage via CB1R-mediated STAT3 phosphorylation," *Molecular Neurobiology*, vol. 53, no. 1, pp. 331–343, 2016.

[33] B. Pál, "Involvement of extrasynaptic glutamate in physiological and pathophysiological changes of neuronal excitability," *Cellular and Molecular Life Sciences*, vol. 75, no. 16, pp. 2917–2949, 2018.

[34] C. M. Miller, P. M. Vespa, D. L. McArthur, D. Hirt, and M. Etchepare, "Frameless stereotactic aspiration and thrombolysis of deep intracerebral hemorrhage is associated with reduced levels of extracellular cerebral glutamate and unchanged lactate pyruvate ratios," *Neurocritical Care*, vol. 6, no. 1, pp. 22–29, 2007.

[35] Y. Zhang, S. Khan, Y. Liu, G. F. Wu, V. W. Yong, and M. Z. Xue, "Oxidative stress following intracerebral hemorrhage: from molecular mechanisms to therapeutic targets," *Frontiers in Immunology*, vol. 13, Article ID 847246, 2022.

[36] A. I. Qureshi, Z. Ali, M. F. K. Suri et al., "Extracellular glutamate and other amino acids in experimental intracerebral hemorrhage: an in vivo microdialysis study," *Critical Care Medicine*, vol. 31, no. 5, pp. 1482–1489, 2003.

[37] G. Wu, L. Wang, F. Wang, A. Feng, and F. Sheng, "Minimally invasive procedures for intracerebral hematoma evacuation in early stages decrease perihematomal glutamate level and improve neurological function in a rabbit model of ICH," *Brain Research*, vol. 1492, pp. 140–147, 2013.

[38] J. E. Chatterton, M. Awobuluyi, L. S. Premkumar et al., "Excitatory glycine receptors containing the NR3 family of NMDA receptor subunits," *Nature*, vol. 415, no. 6873, pp. 793–798, 2002.

[39] D. M. Stanca, I. C. Mărginean, O. Sori ău et al., "GFAP and antibodies against NMDA receptor subunit NR2 as biomarkers for acute cerebrovascular diseases," *Journal of Cellular and Molecular Medicine*, vol. 19, no. 9, pp. 2253–2261, 2015.

[40] C. Wang, Y. Wei, Y. Yuan et al., "The role of PI3K-mediated AMPA receptor changes in post-conditioning of propofol in brain protection," *BMC Neuroscience*, vol. 20, no. 1, Article ID 51, 2019.

[41] K. Ishida, Y. Kotake, S. Sanoh, and S. Ohta, "Lead-induced ERK activation is mediated by GluR2 non-containing AMPA receptor in cortical neurons," *Biological and Pharmaceutical Bulletin*, vol. 40, no. 3, pp. 303–309, 2017.

[42] S. Chen, Q. Yang, G. Chen, and J. H. Zhang, "An update on inflammation in the acute phase of intracerebral hemorrhage," *Translational Stroke Research*, vol. 6, no. 1, pp. 4–8, 2015.

[43] J. Liu, Z. Zhu, and G. K.-K. Leung, "Erythrophagocytosis by microglia/macrophage in intracerebral hemorrhage: from mechanisms to translation." *Frontiers in Cellular Neuroscience*, vol. 16, Article ID 818602, 2022.

[44] Z. Zhang, Z. Zhang, H. Lu, Q. Yang, H. Wu, and J. Wang, "Microglial polarization and inflammatory mediators after intracerebral hemorrhage," *Molecular Neurobiology*, vol. 54, no. 3, pp. 1874–1886, 2017.

[45] S. Chen, L. Zhao, P. Sherchan et al., "Activation of melanocortin receptor 4 with RO27-3225 attenuates neuroinflammation through AMPK/JNK/p38 MAPK pathway after intracerebral hemorrhage in mice," *Journal of Neuroinflammation*, vol. 15, no. 1, Article ID 106, 2018.

[46] X. Jie, X. Li, J.-Q. Song, D. Wang, and J.-H. Wang, "Anti-inflammatory and autonomic effects of electroacupuncture in a rat model of diet-induced obesity," *Acupuncture in Medicine*, vol. 36, no. 2, pp. 103–109, 2018.

[47] R. Torres-Rosas, G. Yehia, G. Peña et al., "Dopamine mediates vagal modulation of the immune system by electroacupuncture," *Nature Medicine*, vol. 20, no. 3, pp. 291–295, 2014.

[48] J. Liu, C. Li, H. Peng et al., "Electroacupuncture attenuates learning and memory impairment via activation of α7nAChR-mediated anti-inflammatory activity in focal cerebral ischemia/reperfusion injured rats," *Experimental and Therapeutic Medicine*, vol. 14, no. 2, pp. 939–946, 2017.

[49] Q.-B. Zhou, Y.-L. Jin, Q. Jia et al., "Baicalin attenuates brain edema in a rat model of intracerebral hemorrhage," *Inflammation*, vol. 37, no. 1, pp. 107–115, 2014.

[50] S. Chen, J. Peng, P. Sherchan et al., "TREM2 activation attenuates neuroinflammation and neuronal apoptosis via PI3K/Akt pathway after intracerebral hemorrhage in mice," *Journal of Neuroinflammation*, vol. 17, no. 1, Article ID 168, 2020.

[51] D.-Z. Liu and F. R. Sharp, "Excitatory and mitogenic signaling in cell death, blood–brain barrier breakdown, and BBB repair after intracerebral hemorrhage," *Translational Stroke Research*, vol. 3, no. S1, pp. 62–69, 2012.

[52] Q. Li, X. Lan, X. Han et al., "Microglia-derived interleukin-10 accelerates post-intracerebral hemorrhage hematoma clearance by regulating CD36," *Brain, Behavior, and Immunity*, vol. 94, pp. 437–457, 2021.

[53] Y. Yao and S. E. Tsirka, "The CCL2-CCR2 system affects the progression and clearance of intracerebral hemorrhage," *Glia*, vol. 60, no. 6, pp. 908–918, 2012.

[54] X. Lan, X. Han, Q. Li, Q.-W. Yang, and J. Wang, "Modulators of microglial activation and polarization after intracerebral haemorrhage," *Nature Reviews Neurology*, vol. 13, no. 7, pp. 420–433, 2017.

[55] M. Ohnishi, T. Kai, Y. Shimizu et al., "Gadolinium causes M1 and M2 microglial apoptosis after intracerebral haemorrhage and exerts acute neuroprotective effects," *Journal of Pharmacy and Pharmacology*, vol. 72, no. 5, pp. 709–718, 2020.

[56] D. Xu, Q. Gao, F. Wang et al., "Sphingosine-1-phosphate receptor 3 is implicated in BBB injury via the CCL2-CCR2 axis following acute intracerebral hemorrhage," *CNS Neuroscience & Therapeutics*, vol. 27, no. 6, pp. 674–686, 2021.